Influence of Wax Inhibitor Molecular Weight:

Part 1. Fractionation and Effect on Crystallization of Polydisperse Waxes.

Jost Ruwoldt[1*], Muh Kurniawan[1,2], Geir Humborstad Sørland[1], Sébastien Simon[1], Johan Sjöblom[1]

[1]Ugelstad Laboratory, Department of Chemical Engineering, NTNU, N-7491 Trondheim, Norway

[2]Research and Development Center for Oil and Gas "LEMIGAS", Jakarta 12230, Indonesia

[*]Corresponding author e-mail: jost.ruwoldt@ntnu.no

Keywords: Wax inhibitor, pour point depressant, wax crystallization, waxy crude oil, flow assurance

Abstract

The molecular weight distribution of four wax inhibitors was modified by either stepwise precipitation or ultrasonic disintegration, and the effect of the obtained inhibitor fractions on wax crystallization was studied. Stepwise precipitation yielded narrower molecular weight distributions as measured by size exclusion chromatography (SEC), whereas ultrasonic disintegration reduced the average molecular weight and increase the polydispersity index. The polymer hydrodynamic radius was mapped using nuclear magnetic resonance (NMR), and showed similar trends as SEC measurements. Wax appearance temperature (WAT) and gelation temperature of three model oils and one crude oil were tested using differential scanning calorimetry (DSC) and rheometry. Changes in molecular weight could improve as well as diminish WAT depression. Waxy gelation temperature showed similar trends as WAT measurements, but the influence of inhibitor molecular weight was more pronounced. The largest change in gelation temperature was measured for the lowest molecular weight fractions

from stepwise precipitation, which had reduced effectiveness on high molecular weight waxes, and improved wax inhibition for lower molecular weight waxes. As cross-polarized microscopy confirmed, the low molecular weight fractions had also lost the ability to distort wax crystal morphology. It was concluded the PPD molecular weight is a parameter that can be used to fine-tune additives to a particular waxy oil, but only after an effective PPD type has been identified.

1. Introduction

During crude oil production, issues due to wax crystallization are among the most commonly faced challenges.[1] Efforts have been made to explore unconventional petroleum sources and harsher environments, i.e. marine deep waters.[2] Such cold environments can cause cooling of crude oil below wax appearance temperature (WAT). Precipitated wax can then build up as deposition layer on pipeline wall during continuous production, leading to pipeline plugging. Other issues associated with crystallized wax include reduced operation efficiency and the formation of high yield strength gels during production stop.[3] To tackle these issues, different wax prevention and remediation measures have been developed. These include thermal insulation and heating (thermal measures), scraping off deposited wax with a pig or wireline cutters (mechanical remediation measures), and the use of pour point depressants (PPDs) and wax inhibitors (chemical prevention measures).[4] Especially the latter has been shown to depress waxy gelling and ensure low viscosity of the crude oil even after wax has crystallized. Much is known about the effect that PPDs have on wax crystallization, however, the precise mechanism of action is not evident.[5] In this study, the influence of PPD molecular weight on wax crystallization is therefore studied as a parameter with importance to flow assurance.

Wax crystallization and waxy gelation works in three steps, which are nucleation, growth, and agglomeration.[6] After the wax crystallization onset (nucleation) wax crystals grow to larger

structures, which can exhibit plate shapes, needle shapes, and malcrystalline masses.[7-8] At a later stage, these crystals interlock, forming volume spanning, three dimensional structures. These gels exhibit complex rheology, such as thixotropy and viscoplasticity.[9] The temperature of solidification can be measured as the pour point or gelation point. The pour point describes the temperature, at which the waxy oil loses its ability to flow freely, and was first defined by ASTM D97.[10] The gelation point is often extracted from rheological measurements, for which both oscillatory and non-oscillatory protocols have been published.[11-12] Waxy gelling and gel properties are influenced by factors such as cooling rate and shear conditions during wax crystallization.[13] Moreover, the composition of wax as well as crude oil plays an important role. Macrocrystalline and microcrystalline waxes are distinguished based on crystal shape, where macrocrystalline wax forms large plate and needle shaped structures, and microcrystalline wax predominantly forms small and compact crystal shapes.[5] Macrocrystalline wax comprises large portions of low molecular weight *n*-alkanes, whereas microcrystalline wax has a high ratio of higher molecular weight *iso*-alkanes. Natural crude oil constituents, such as asphaltenes and resins, can also affect waxy gelling.[14-15]

Wax inhibitors and pour point depressants (PPD) are reported to interact with wax via co-crystallization on wax crystals, and by affecting wax nucleation and solubility.[5] Computer simulations have shown that the polyethylene (PE) backbone or pendant alkyl chains adsorb onto the crystal lattice, causing disruption and decreased growth rate for further paraffin layers added on top of the PPD.[16-17] Such processes can lead to the formation of distorted and more compact crystal masses, which consequently have lower propensity to overlap, effectively delaying gelling and reducing the strength of formed gels.[8] Above WAT, PE-polypropylene (PEP) polymers have been shown to self-assemble into micelle-like aggregates that have a crystalline core with surrounding brushes composed of single alkane chains.[18-19] These can then facilitate wax nucleation, which creates a larger number of subcritical size wax nuclei

(polynucleation), which can furthermore cause the formation of smaller and more abundant wax crystals.[5, 20-21] Because of a lower average crystal size, the overall gel structure exhibits lower structural stability and therefore reduced strength. Moreover, PPD beneficiation has been reported to lower WAT and the total amount of precipitated wax.[20, 22-24] WAT depression is attributed with favorable van der Waals interactions between paraffin wax and PPD alkyl moieties.[5] However, PPDs were also reported to increase wax dissolution temperature,[23] which suggests that WAT depression might be a kinetic effect rather than improve thermodynamic solubility.

Different types of PPDs exist, which can be grouped into ethylene polymers and copolymers, comb polymers, and nanoparticle composites.[5] Ethylene copolymers are made of a PE backbone with additional amorphous moieties, such as polybutene (PB) or polyethylenepropylene (PEP). The most commonly used copolymer for wax inhibition is ethylene vinyl-acetate copolymer (EVA).[3] Comb polymers are usually synthesized from (meth)acrylic acid, maleic anhydride or both.[3, 25] According polymers, i.e. polyacrylate (PA) or poly(maleic anhydride amide co-α-olefin), are attributed with improved inhibition performance as a result of their pendant alkyl-chains interacting with wax.[3, 5, 26] Nanoparticles have been used in combination with PPD additives to enhance the effect of the latter. According technologies are still subject to research, but chemistries such as as poly(octadecyl acrylate) on nanosilica, EVA on nanosilica, and EVA on polymethylsilsesquioxane microsphere have shown good wax inhibition efficiency.[27-30]

PPD molecular weight has been mentioned as one of the parameters influencing wax inhibition performance.[5-6, 31] For example, reducing the molecular weight of dialkyl fumarate-vinyl acetate copolymers could enhance as well as diminish pour point depression, depending on the waxy crude oil.[31] PPD polymers with too low molecular weight were stated to not exhibit high enough molecular volume to effectively disrupt wax crystal growth.[32] Too high molecular

weight on the other hand can promote PPD-PPD or PPD-wax interactions that aggravate waxy gelling. Moreover, the molecular weight can affect PPD solubility.[32] This can in turn affect the wax inhibition capabilities, as the most effective wax inhibitors were found to aggregate at the temperature of the wax crystallization event.[20]

The goal of this study is therefore to extend the knowledge about how PPD molecular weight affects wax crystallization. For the same purpose, previous approaches have employed products of different origin and syntheses.[6, 31-32] This study presents an alternative way of testing, by changing the molecular weight distribution of particular PPDs by either stepwise precipitation or by ultrasonic disintegration. In depth characterization of PPDs and according sub-fractions is done with respect to polystyrene (PS) equivalent molecular weight, hydrodynamic radius, and precipitation from pure solvent. The results are then compared with PPD effect on wax crystal morphology, WAT, and gelation temperature in four different waxy oils.

2. Experimental Section

2.1. Materials

A light crude oil (API 47.7°) from the Norwegian continental shelf was used. Atmospheric gas oil (AGO) refined at temperatures below 375 °C from a crude oil was obtained. Primol 352 mineral oil was obtained from ExxonMobil. 5405 and 6805 Sasolwax with a congealing point (ASTM D 938) of 53 – 55 °C and 66 – 70 °C, respectively, were obtained from Sasol, Germany. Solvents used for PPD purification and fractionation include toluene (Sigmaaldrich Norway, 99.8%, anhydrous), *n*-dodecane (Sigmaaldrich Norway, ≥99%, reagent plus), and p-xylene (Sigmaaldrich Norway, ≥99%, anhydrous). PPD characterization was conducted with tetrahydrofuran (THF, VWR Norway, ≥99.7%, HPLC grade), deuterated toluene (Sigmaaldrich, 99.6 atom % D, anhydrous), and *n*-octane (Sigmaaldrich Norway, ≥99.0%, puriss). PPD additives used in this study are listed in Table 1. PPD τ contains > 0.03 wt.%

antioxidant inhibitor and PPD Ω contains 200 – 900 ppm BHT as inhibitor. Calibration standards for HPLC-SEC were obtained as SM-105 Shodex standard kit, which contained ten polystyrene (PS) standards ranging from 1.22 kDa to 270 kDa.

2.2. Sample Preparation

Crude oil was placed in an oven at 60 °C for 1 h and shaken thoroughly prior to sample taking to ensure homogeneity of the sample. Waxy solutions were prepared by first weighing the solids and then adding the required amount of solvent. Prior to usage, solids in these solutions were dissolved by heating the sample vial to at least 20 °C above WAT for at least 30 min. In addition, sonication at temperatures above WAT was used if visual inspection of the sample revealed undissolved PPD additives. Three different model oils, as well as light crude oil spiked with wax were prepared to test the effect of fractionated PPD and are listed in Table *2*.

Prior to fractionation, PPD α and β were purified, as these were originally supplied as blend with petroleum distillate. Toluene was repeatedly added and removed to the PPD in a rotary evaporator at up to 90 °C and 200 mbar. Afterwards, the remaining substance was dried in an oven at 60 °C and ambient pressure for 24 h.

2.3. PPD Fractionation

Two essentially different PPD additives were used in this study, where PPD α and β contain polydisperse polymer of proprietary chemistry, and PPD τ and represent pure polymer of known composition. Two different fractionation procedures were used, which are described below.

2.3.1. Fractionation by Stepwise Precipitation

Fractionation of PPD α and β was carried out by precipitating the PPD from a dodecane solvent at 15 °C. PPD solutions were prepared at a concentration of 1 wt%. The solution was loaded

into a glass centrifuge tube, which was submerged in a water bath for 2 hours to induce PPD precipitation. The sample was transferred to a centrifuge of type Multifuge X3R from Thermo Scientific, was kept isothermal at the fractionation temperature. Centrifugation was done for a total of 90 minutes at 3000 rpm giving a centrifugal force of 1962 g at the bottom of the centrifuge tube. The solid phase was recovered by decanting the liquid phase and subsequent solvent evaporation under nitrogen atmosphere at 122°C, yielding PPD α high and PPD β high, respectively. In case of PPD α, the procedure was repeated at 8 °C to recover the solids of a second fraction (PPD α mid). Afterwards, the decanted liquid phase also underwent solvent removal by evaporation under nitrogen atmosphere at 122 °C to purify the second (PPD β low) or third fraction (PPD α low).

2.3.2. Fractionation by Ultrasonic Disintegration

50 ml solutions of 2 g/l PPD τ or Ω in p-xylene were prepared. Ultrasonic disintegration was conducted using a Digital Sonifier 450 CE from BRANSON Ultrasonics Corporation. The disrupter horn (fitted with flat tip) was immersed one third into the sample. The sample vial itself was immersed in ice-water to prevent excessive heating. Sonication was performed at 60 % of the maximum power of 400 W in 15 min intervals. Short ultrasonic treatment refers to a single 15 min interval (PPD τ short US) and long treatment used four intervals of in total 60 min (PPD τ long US, PPD Ω long US).

2.4. HPLC-SEC

The molecular weight distribution of the PPDs was determined via HPLC employing a series of two packed bed columns, which are KF-804 followed by KF-803 from Shodex, Japan. These allowed separation of polymer with a lower exclusion limit of 1 kDa and a higher exclusion limit of 400 kDa polystyrene (PS) equivalent. The detector was a Shimadzu SPD-20A UV-detector measuring at a wavelength of 220 nm. THF was used as bulk solvent at a flow rate of

1 mL/min, and calibration was performed using five Shodex SM-105 polystyrene (PS) standards, ranging from 1.22 to 326 kDa. Injections of 20 µL were done with a sample concentration of 1000 ppm and a calibration standard concentration of 1 g/L. In case of PPD Ω and according sub-fractions, the sample concentration was doubled to 2000 ppm.

2.5. NMR-DOSY

Diffusion ordered spectroscopy (DOSY) provides a tool that may correlate chemical shift information with the molecular mobility of the sample.[33-34] Pulsed field gradient stimulated echo (PFGSTE) is looped once during the rapid DOSY sequence, as illustrated in Figure 1. Here, g refers to the applied gradient strength, $GS1$ and $GS2$ are the spoiler gradient pulses, and SRD is the spoiler recovery delay.

The sequence is rapid due to the spoiler sequence prior to the third 90 degree excitation pulse, as it bypasses the need for waiting 5 times T_1 for thermal recovery of the NMR signal. The attenuation $I(\upsilon)$ of the Fourier transformed FID for a multi exponential system at a given frequency υ is provided in equation (1), where γ is the gyromagnetic ratio, ρ_i is the weighting factor of region i, D^i is the diffusion coefficient, and T_1^i is the longitudinal relaxation time.

$$I(\upsilon) = I_0(\upsilon) \sum_i \rho_i \left(1 - \exp\left(\frac{SRD}{T_1^i}\right)\right) \exp\left(-2\gamma^2 g^2 \delta^2 D^i \left(\Delta - \frac{\delta}{3}\right)\right) \quad (1)$$

By fixing SRD and incrementing the gradient strength only, a set of FID's as a function of gradient strength is produced. After a Fourier transform (FT) of the FID, the spectra are subjected to a one dimensional inverse Laplace routine,[35] resulting in a distribution of diffusion coefficients for each frequency point in the spectra. From equation (1) it can be seen that a change in SRD will lead to different contributions from components with different T_1 relaxation times. This can be used for partial solvent suppression, as one usually wants to study macromolecules with short T_1 that are dissolved in a solvent having longer T_1. The PFGSTE

part of the sequence is run twice to compensate for convection artefacts.[36] If not, the results could vary depending on solvent viscosity and inner diameter of the sample tubes as well. Figure 2 shows a DOSY spectrum from sample containing macromolecules dissolved in deuterated toluene. The DOSY spectra of all measurements are provided in the supplementary material.

Using Stokes-Einstein relation given in equation (2), the diffusion coefficient D and Boltzmann constant k_B can be used to further compute the hydrodynamic radius R_H.[37]

$$R_H = \frac{k_B T}{6\pi\eta D} \tag{2}$$

As the DOSY returns a distribution of diffusion coefficients (projection along the vertical axis in Figure 2), a distribution of hydrodynamic radii may also be produced from according data. All samples were measured at 1000 ppm PPD in deuterated toluene at 296 K. Due to low PPD concentration, negligible influence on solvent viscosity was assumed for hydrodynamic radius calculations.

2.6. Differential Scanning Calorimetry (DSC)

DSC experiments were conducted on a Q2000 from TA Instruments. Calibration of the instrument was done by measuring the heat and temperature of melting pure indium. 15 to 30 mg sample were filled into Tzero Hermetic Pans and sealed hermetically. Experiments consisted of heating to 80 °C (pure PPD in *n*-octane or crude oil samples), or 100 – 110 °C (model oil A, model oil B, and model oil C) for a duration of 5 – 20 min to remove all thermal history. After that quick cooling to approximately 40 °C above WAT was done, before the measurement commenced and a cooling rate of 1 °C/min was applied. Cooling and heating cycles were repeated up to three times, yielding up to four measurements per loaded sample pan. A series of measurements was only accepted if the repeating cycles showed both

qualitative and quantitative reproducibility. The mass of loaded sample pans before and after DSC measurement was also used to check if the sample pan remained hermetically sealed and no solvent loss occured. WAT was determined according to a previously published procedure.[38] In this procedure, the heat flow before crystallization onset is fitted by a straight line on a temperature interval of 15 °C and a confidence interval is calculated as 3.291 times the standard deviation of data around the straight line approximation. The WAT is defined as the highest temperature, below which three consecutive points are outside the confidence interval.

2.7. Rheometry and Gelation Point

Rheological experiments were conducted on a Physica 301 from Anton Paar, Austria. The rheometer was equipped with cone and plate geometry (2° cone inclination, 4 cm cone diameter), which had been sandblasted to provide roughness and prevent slippage. The geometry used a gap size of 0.17 mm. The hot sample was loaded into the geometry, which was preheated at least 10 °C above WAT. Cooling at a rate of 1 °C/min was subsequently applied and the measurement commenced by imposing an oscillation shear stress of 1.2 Pa at a frequency of 1 Hz. The gelation point was defined as the highest temperature, at which storage (G') and loss modulus (G") are equal. In practice, this temperature was interpolated linearly from data directly above and below the intersection of the two moduli. The measuring interval was set to 15 s. Temperature cycling could be done by heating to 100 °C for 15 min (model oil A) or 110 °C for 20 min (model oil B). Due to low vapor pressure of the solvent Primol 352, temperature cycling showed complete removal of thermal history with no apparent solvent loss and good data reproducibility. In case of model oil C and crude oil, no thermal cycling was done and each measurement was conducted with newly loaded sample.

2.8. Cross-Polarized Microscopy (CPM)

CPM experiments were conducted with a Nikon Eclipse ME600 microscope fitted with CoolSNAP-Pro camera from Media Cybernetics and cross-polarization filters. Temperature control was done via PE 94 and LTS-120E Peltier system from Linkham, United Kingdom. Samples were filled into glass capillaries with a cross-section of 1 x 0.05 mm (width x height), sealed at the ends using 3M Scotch cyanoacrylate glue, and fixed in place on a microscope slide. An air bubble was kept between sample and glue to prevent contamination. The temperature protocol consisted of heating to 60 °C (model oil A, model oil C, crude oil) or 80 °C (model oil B) and keeping isothermal for 15 min. Fast cooling to approximately 20 °C above WAT could be done, and a constant cooling rate of 1 °C/min was subsequently applied. Images were taken after equilibrating isothermally for at least 30 min.

3. Results and Discussion

Results are presented in the following, which discuss waxy oil characteristics, PPD fractionation and characterization, and furthermore the effect of PPD additives on WAT and gelation point.

3.1. Waxy oil characteristics

DSC and CPM experiments were conducted to provide characteristics of the waxy oils before utilizing these to test PPD effect on wax crystallization. DSC experiments assessed the amount of wax contained in Primol 352, AGO, and crude oil. Results are shown in Figure 3 together with pure waxes in *n*-octane. As can be seen, all oils contain measurable portions of wax with a WAT below ambient conditions. Wax contents were estimated using the procedure by Chen et al., in which the DSC signal is integrated linearly from WAT to -20 °C.[39] Averaged over four measurements, the amount of wax was estimated to be 1.0 wt% (Primol 352), 2.3 wt% (AGO), and 1.4 (light crude oil). These values have to be interpreted with care, however, since

DSC is not a replacement for more accurate methods that assess e.g. the actual sample composition.

The largest portion of 5405 Sasolwax (> 75 wt%) is made up by *n*-alkanes with a molecular weight between C_{21} and C_{35}, as has been published by other authors.[40] As can also be seen in Figure 3, 6805 Sasolwax has the wax crystallization onset approximately 15 °C higher than 5405 Sasolwax and exhibits a similar peak broadness. The average molecular weight of 6805 Sasolwax therefore appears higher than 5405 Sasolwax with a similar polydispersity index. Concurrent observations were made by DOSY-NMR measurements as shown in Figure 4. The hydrodynamic radius distribution of 6805 Sasolwax shows the same shape as 5405 Sasolwax, only at higher hydrodynamic radii. The distribution of *n*-octacosane is in comparison narrower with a higher peak maximum, which concurs with the trend expected for a single *n*-alkane.

Both waxes are macrocrystalline in nature, as can be seen in Figure 5. Model oil B (10 wt% Sasolwax 6805) and model oil C (5 wt% 5405 Sasolwax) show large crystal structures that appear plate or needle shaped with dimensions of up to 20 µm, which are sometimes co-joined in a stearic center. In model oil A (5 wt% 5405 Sasolwax), the wax crystallizes with similar and shows smaller crystals in addition that are considerably smaller than for model oil B and model oil C. In crude oil (10 wt% 5405 Sasolwax) the wax crystals are shaped more round, where individual straight lines can be clustered around a more compact center. The difference in crystal morphology of crude oil can be linked to natural crude oil components that are PPD-active, such as asphaltenes and resins.[15, 41]

3.2. PPD Fractionation and Characterization

Fractionation by stepwise precipitation of PPD α had a normed yield of 16.5 wt% (PPD α low), 38.3 wt% (PPD α mid), and 45.2 wt% (PPD α high) at a loss percentage of 5.3 wt%. Mass

balancing the fractionation of PPD β yielded 28.6 wt% (PPD β low), and 71.4 wt% (PPD β high) at a loss percentage of 3.1 wt%. Losses are attributed mostly with PPD stuck inside the used glassware, as each PPD had undergone solvent removal before fractionation. Fractionation by ultrasonic disintegration introduced impurities showing as discoloration of the solvent, which are likely cause by erosion of the disruptor horn tip. Direct contact with the disruptor horn was necessary to induce polymer scission, and the impurities could not be removed by filtration through a 0.45 μm Millipore filter. Mass balancing the fractions obtained for PPD τ and PPD Ω, weight increases of 5 – 30 wt% were noted. A separate discussion of the effect of impurities on waxy gelation is provided in section 3.3.1.

3.2.1. HPLC-SEC molecular weight

Chromatograms of HPLC-SEC experiments are plotted in Figure 6. Molecular weight of the lowest (1200 g/mol) and highest (326 000 g/mol) calibration standard are marked in addition, as the region between these accounts for selective permeation and thereby accurate chromatographic separation. The exclusion limit was stated by the column manufacturer as 400 000 g/mol (PS in THF). Trial runs on the KF-803 column with toluene (92.14 g/mol) showed that retention of this component was still coinciding with the calibration line. Both the sub-fractions of PPD α and PPD β illustrate that separation yielded products with narrower molecular weight distributions. The differences between PPD α mid and PPD α high appear small by qualitative comparison. Large differences can be noted on the other hand for PPD α low, as well as for the two sub-fractions of PPD β. Ultrasonic treatment reduced both the maximum and average molecular weight of PPD Ω. In case of PPD τ, ultrasonic disintegration reduced the size of the peak at 140 kDa and produced several distinct fractions of lower molecular weight.

HPLC chromatograms were converted to number average (M_n) and weight average (M_w) molecular weight using equations (3) and (4). Here M_i refers to the PS-equivalent molecular weight at measurement point i. N_i is the amount of substance in moles, which is proportional to the peak area A_i divided by M_i. Trapezoidal integration is used to calculate area A_i for each data increment.

$$M_n = \frac{\sum_i N_i M_i}{\sum_i N_i} = \frac{\sum_i A_i}{\sum_i \frac{A_i}{M_i}} \tag{3}$$

$$M_w = \frac{\sum_i N_i M_i^2}{\sum_i N_i M_i} = \frac{\sum_i A_i M_i}{\sum_i A_i} \tag{4}$$

Signal return to the baseline marked both the upper integration boundary close to the 326 kDa standard and the lower integration boundary between 1.2 – 0.2 kDa. Results are listed in Table 3. As can be seen, fractionation by stepwise precipitation yielded sub-fractions with lower polydispersity index. Moreover, the number and mass average molecular weight of the highest fraction (PPD α high and PPD β high) is larger than that of the respective parent PPD. Analogously, the lowest fraction (PPD α low and PPD β low) exhibits lower molecular weight averages. Moreover, the molecular weight change is more pronounced for the lowest fractions, which can be explained by the fact that these comprise a smaller fraction of the total parent PPD. Fractionation by ultrasonic disintegration in both cases reduced the molecular weight and increased the polydispersity index. This decrease was progressive in case of PPD τ, but more rapid in case of PPD Ω. It has to be noted that molecular weight averages are to some extent only estimates, as part of the integrated signal could lay outside the calibration region.

3.2.2. PPD hydrodynamic radius by NMR-DOSY

Hydrodynamic radii as depicted in Figure 7 show similar trends as the molecular weight distributions in section 3.2.1. Both PPD α and PPD β have a broader distribution before

fractionation. After fractionation, the hydrodynamic radius of these is narrower and the average radius increases as fractionation temperature goes up. Similar as in HPLC measurements, the difference between PPD α mid and PPD α high is little. PPD β exhibits a bimodal distribution, which is also visible in case of PPD β high. PPD β low shows no bimodality and has the peak maximum right in between the two local maxima of PPD β. The hydrodynamic radius of PPD τ and its fractions is narrower than for other PPDs, which is in accordance with a lower polydispersity index for this PPD, also. The distribution of PPD τ was progressively shifted to lower hydrodynamic radii after ultrasonic treatment, and a second peak at approximately 2 Å appeared. The hydrodynamic radius distribution of PPD Ω did not change after sonication. This trend is in contradiction with the results from HPLC-SEC in Figure 6, which clearly show a reduction of PPD Ω molecular weight after ultrasonic treatment. This difference could be explained by the fact that HPLC measurements used solutions in THF, whereas NMR-DOSY was performed on solutions in deuterated toluene. The folding of polymers and self-association behavior could be solvent dependent. Moreover, shear is applied to the sample during SEC measurements, which could lead to the breakdown of weakly bound aggregates, whereas NMR measurements are performed on quiescent samples.

The volume based average radius $\overline{R_v}$ was computed by equation (5) and from the hydrodynamic radius distribution of Figure 7, where w_i refers to the normalized ratio of PPD at radius R_i. The computed average hydrodynamic radii are listed in Table 4. These confirm trends that have been pointed out by the qualitative graphs of Figure 7.

$$\overline{R_v} = w_i R_i \tag{5}$$

3.2.3. PPD precipitation from pure solvent

Precipitation of pure PPD in *n*-octane is plotted in Figure 8. As can be seen, the crystallization enthalpy of PPD Ω and PPD τ is approximately one magnitude lower than for PPD α and

PPD β. Both PPD α and PPD β exhibit multiple crystallization peaks. For PPD α, peak maxima are recorded at approximately 10 °C, -17 °C, and -23 °C. The two peaks at lower temperature appear to be amplified for PPD α low with a reduction of the previously largest peak at higher temperatures. PPD α mid and PPD α high exhibit mainly this peak with an additional smaller peak slightly above -25 °C. Overall, the precipitation temperature of the main precipitation peak around -5 to 10 °C appears to be affected much less by fractionating PPD α than peaks at lower temperatures. A similar case can be seen for PPD β, which displays one peak with a maximum at 15 °C, the largest peak at 9 °C, and a comparably broad peak with a maximum at -10 °C. PPD β low appears to have only the two peaks at lower temperatures and PPD β high the two at higher temperatures. As fractionation was based on precipitation at certain temperatures, it becomes evident that this procedure isolated PPD with specific precipitation regions. Attributing these to PPD molecular weight as studied in section 3.2.1 is more difficult, because HPLC graphs do not show such a trimodal molecular weight distribution. On the other hand, precipitation peaks PPD α and PPD β fractions at temperatures below -5 °C could be due to unreacted monomer or remaining solvent, which did not show in HPLC graphs due to a too low molecular weight.

Both PPD Ω and PPD τ exhibit an increase in precipitation temperature after ultrasonic treatment. In addition to the graphs shown, each of these additives was tested with added impurities. DSC of PPD τ with impurities showed identical precipitation behavior as pure PPD τ. However, the heat flow of PPD Ω with impurities was shifted to higher temperature in the same way as PPD Ω long US. A possible explanation could be that the impurities serve as nucleation sites, inducing crystallization at slightly elevated temperatures. The overall trend for PPD τ suggests that sonication could have lowered PPD solubility, yielding a higher precipitation onset temperature. Another possible explanation could be that precipitation kinetics are faster due to a lower molecular weight. A peak smaller than the main peak is visible

at approximately -5 °C, which is remains at the same temperature for PPD τ and all sub-fractions. This peak could indicate that the actual solubility limit is up to 15 °C higher than the onset of the main peak. However, such conclusion cannot be made with certainty due to low signal to noise ratios.

In conclusion, the precipitation behavior of fractions obtained from stepwise precipitation is in good agreement with HPLC and NMR results. Precipitation of PPDs treated by ultrasonic disintegration shows atypical behaviour, which could partially be explained by the impurities in the samples.

3.3. PPD effect on wax crystallization

Preliminary testing with different PPD concentrations had shown that 500 ppm PPD in waxy oil induce well-measurable WAT and gelation point depression, while no overdosing effects could be detected. This concentration was therefore used for the entire performance evaluation, to provide consistency and comparability of the measured data.

3.3.1. Influence of impurities from ultrasonic disintegration

Ultrasonic disintegration introduced impurities as mentioned in section 3.2. Direct contact with the disrupter horn was necessary, however, to obtain the required energy input for PPD scission. Cleaning protocols were in place, so the origin of these impurities is not contamination from previous sonication experiments. Instead, tip erosion is the suspected origin of impurities, as this is a common concomitant phenomena in high energy ultrasound.

The effect of impurities on wax crystallization was studied systematically. 50 ml of *p*-xylene without PPD were sonicated for 15 min to collect impurities without PPD treatment. A 2 g/l solution of PPD τ and PPD Ω was subsequently prepared with the *p*-xylene containing impurities. The PPD solutions were further processed as had been done with sonicated PPD. Effect of PPD additives with and without impurities on WAT and gelation point is shown in

Figure 9. Individual measurements could be skewed towards one side, e.g. lower WAT for pure PPD Ω in crude oil, and higher gelation point for PPD τ with impurities in model oil A. However, none of the two attributes exhibited an overall dominant effect on WAT or gelation point.

The effect of impurities was also investigate using CPM imaging. Example images are displayed in Figure 10. In case of PPD τ, no difference between PPD with and without impurities was visible. Both changed wax crystal morphology to smaller, more compact, and finely dispersed particles. The effect of PPD Ω on wax crystallization was the formation of larger and compact crystals that exhibited morphologies, which were distorted and amorphous in nature. As can be seen in Figure 10, smaller crystals are visible in addition when PPD Ω with impurities was added. This suggests that the impurities could induce polynucleation in addition by serving as nucleation sites. Nanoparticle-PPD composites have been stated to function in a similar way, as these can lead to the formation of compact and amorphous aggregates by serving as nucleation sites.[29, 42] The action of PPDs with impurities from ultrasonic disintegration is not directed towards performance enhancement in this case, as the PPDs have not been chemically bound on the impurities. In conclusion, the presence of impurities from ultrasonic disintegration might facilitate wax nucleation, but at the same time no significant influence on WAT and gelation point could be detected.

3.3.2. PPD effect on WAT and wax precipitation

The effect of PPD fractionation on wax precipitation was investigated by DSC. According WAT values are plotted in Figure 11. Industrial wax inhibitors (PPD α and PPD β) and their fractions showed the largest effect on WAT of both model oil A and model oil C. PPD α and according fractions showed an increase in WAT in crude oil. The effect of PPD β and PPD Ω (both EVA based) on delaying wax crystallization in crude oil was largest. PPD τ had the

smallest effect on WAT of all PPDs tested. According fractions (PPD τ short and long US) exhibited slightly improved WAT depression for model oil A, but showed adverse effects in crude oil. General trends were given e.g. by PPD α low, which was higher or equal in WAT to its parent PPD for all waxy oils. A similar trend can be seen for PPD β low. The largest difference is apparent from PPD Ω long US in crude oil, which reduced WAT by 3 °C more than PPD Ω.

As can be seen in Figure 12, PPD additives could delay the wax crystallization onset, as well as change the heat flow profile during wax crystallization. Crystallization onset of model oil A, model oil C, and crude oil (all containing 5405 Sasolwax) was marked by a gradual increase of the heat signal. This gradual increase was shifted to lower temperatures in case of PPD α and according fractions in model oil C, PPD τ and according fractions in model oil A and C, as well as PPD Ω and PPD Ω long US in model oil A. Larger WAT reduction was often accompanied by a sharp signal peak at crystallization onset. Examples where this effect is strongly pronounced include PPD β high in model oil A, model oil B, and crude oil, as well as PPD Ω and PPD Ω long US in crude oil. Heat flow changes below -10 °C can be attributed mainly to crystallization of the solvent matrix and showed little change as a result of PPD addition. Fractionated PPDs change in particular occurrence and shape of local maxima that can be found in addition to the wax crystallization peak. The main wax crystallization peak is located between 0 °C and 30 °C (model oil A, model oil C, crude oil) or 0 °C and 50 °C (model oil B), respectively. For example in model oil A, the additional local maxima are visible for both PPD α and PPD β at approximately 26 °C. These local maxima are not visible for PPD α low or PPD β low, but they are visible with enhanced magnitude in case of PPD α high and PPD β high. At the same time, WAT values for PPD α low and PPD β low are in comparison higher. The same observation is made for model oil B, where PPD α high and PPD β high account for an increase in the global maximum right after wax crystallization onset. It appears

that PPD fractionation has removed a portion of PPD that is more active at wax crystallization onset. Conversely, it can be concluded that it is majorly the higher molecular weight fraction of these PPDs that is causing delayed wax crystallization.

3.3.3. PPD effect on wax crystallization and waxy gelation

The effect of different PPDs and their sub-fractions on waxy gelation was investigated by rheometry, whereas crystal morphology was studied by CPM. Results from CPM imaging of model oil A are exemplarily shown in Figure 13. For comparison, uninhibited model oil A is displayed in Figure 5. Fractionation of PPD α and PPD β yielded slight changes to crystal morphology. The crystal shape of PPD α and PPD α high is more amorphous, whereas PPD α low and PPD α mid exhibit a larger fraction of linear shapes. The high molecular weight fraction of PPD α therefore appears to induce a larger degree of crystal distortion. Similar crystal shapes as for PPD α were seen for PPD β, but the individual crystal dimensions are smaller in case of PPD β low. Ultrasonic disintegration of PPD τ and PPD Ω yielded little change with respect to wax crystal morphology. Model oil A with PPD τ or PPD Ω show small and finely dispersed wax crystals, which are in close proximity to each other. All PPDs induced some degree of crystal distortion with respect to the uninhibited model oil A of Figure 5. However, it appears that the individual crystal shape and size is mostly determined by the type of PPD and variations are not as pronounced among the sub-fractions.

The imposed shear stress during gelation point measurements was set to 1.2 Pa, which represents the higher end of procedures published by other authors.[12, 43] Increasing the imposed shear stress results in a lower gelation temperature observed. Also, exceeding the linear viscoelastic regime can result in G' and G" to lose their physical meaning.[44] The presented gelation temperatures are therefore underestimates of the gelation temperature obtained by quiescent cooling. However, a high imposed shear stress represents the conditions during

continuous pipeline transport of crude oil more accurately. Moreover, preliminary tests had shown that higher imposed shear stress also leads to larger differences in gelation temperature as a result of PPD beneficiation. The presented method therefore represents a procedure optimized to map the influence of PPD fractionation on waxy gelation.

Exemplary data used for gelation point determination is plotted in Figure 14. Uninhibited model oils attained gelation point approximately 5 – 10 °C after WAT and shortly after the storage modulus started increasing in value. PPD beneficiated oils exhibited slower and more gradual increase in storage and loss modulus.

Average gelation points for every sample are plotted in Figure 15. Good PPD performance is attributed with a large decrease in gelation point due to PPD beneficiation. General trends correlate to some extent with average WAT of Figure 11, meaning that PPD additives inducing greater WAT depression often also resulted in greater gelation point depression. PPD α and PPD β were most effective in model oil A and model oil C. PPD τ had the worst overall performance and fractionation of PPD τ showed improved effect only in crude oil. PPD Ω was less effective in model oil A and model oil C, but showed good performance for model oil B and the best overall performance for crude oil. CPM images of Figure 13 would suggest a high impact of PPD τ and PPD Ω on lowering the gelation temperature of model A, because addition of these led to the formation of small and finely dispersed crystals. Even though crystal dimensions were reduced, the gelation point is close to the gelation temperature of the uninhibited case. This suggests that PPD τ and PPD Ω did not affect crystal interlocking to an extent, where the formation of a cohesive crystal-network could be prevented. Measurements were generally reproducible within a certain margin of error. Data has to be interpreted with care when considering PPD β and PPD β high in model oil B, since the gelation temperature exhibits large scattering. It appears that PPD activity was stronger around and below upper gelation temperature. If measurements went below a certain threshold temperature, continued

shear and co-crystallization of PPD β and PPD β high would delay the gelation point by another 30 – 40 °C.

Fractionation by ultrasonic disintegration could both aggravate and improve PPD performance, but no overall trend was found. In contrast to that, PPD fractionation by stepwise precipitation showed a distinct trend for the lowest molecular weight fractions, PPD α low and PPD β low. These would induce larger gelation point depression than the respective parent PPD in model oil A and model oil C. In crude oil, PPD β low furthermore depressed the gelation temperature below -20 °C. In model oil B, which contained wax with a higher average molecular weight than model oil A and model oil C, the gelation point depression of PPD α low and PPD β low was lower than for the parent PPD. This effect could also be seen in CPM imaging. As depicted in Figure 16, addition of PPD α would result in the formation of compact crystal aggregates in model oil B, which were mostly crumbled and amorphous in nature. Addition of PPD α low in comparison resulted in the formation of a dense crystal network with individual crystals overlapping and intermeshing. Crystal agglomeration to interconnected structures of higher molecular weight wax could therefore not be prevented, if the high molecular weight fraction of a PPD was removed. It can therefore be concluded that PPD molecular weight can be adjusted to closely match the precipitation region of the wax. This can improve wax inhibition efficiency, while incorrect adjustment can diminish the effect of a PPD.

4. Conclusion

In this article, four PPD additives were fractionated by either stepwise precipitation or ultrasonic disintegration to produce sub fractions with different molecular weight. These were subsequently characterized via HPLC SEC, NMR DOSY, and DSC to study the change in molecular weight distribution, hydrodynamic radius, and precipitation from n octane. The effect of PPDs and their sub fractions on WAT and gelation point of three model waxy oils and

one crude oil was further investigated by DSC and rheometry. In addition, the change in wax crystal morphologies was studied using CPM.

Stepwise precipitation yielded sub fractions of PPD α and PPD β with increased and reduced average molecular weight and lower polydispersity index as compared to the parent PPD. Similar trends were seen in the hydrodynamic radius distributions and by pure PPD precipitation in octane. Ultrasonic disintegration reduced the average molecular weight of PPD τ and PPD Ω, while increasing the polydispersity index.

The lowest molecular weight fractions obtained by stepwise precipitation showed reduced effect on delaying waxy gelation of high molecular weight wax. This reduced efficiency was also observed in CPM imaging, where according PPDs lost the ability to induce wax crystal distortion. The highest molecular weight fractions in contrast could enhance exothermic crystallization peaks right below crystallization onset, which were observed for two of the model oils. Ultrasonic disintegration could enhance gelation point depression of PPD τ in crude oil. In model oils, ultrasonic treatment of PPD could improve as well as diminish wax inhibition, but with overall less effect. On average, PPD effect on WAT and gelation point was dictated more by the type and functional groups of a particular PPD than by its molecular weight.

In conclusion, PPD molecular weight is one of the parameters that are influencing additive effect on wax crystallization. However, the ability to induce wax crystal distortion with beneficial influence on crude oil flow ability are properties that were largely dictated by the type of PPD. Molecular weight is therefore a parameter that can be used to optimize a PPD to a particular waxy oil, but only at a later stage during additive development.

Acknowledgements

This work was carried out as a part of SUBPRO, a Research-based Innovation Centre within Subsea Production and Processing. The authors gratefully acknowledge the financial support from SUBPRO, which is financed by the Research Council of Norway, major industry partners and NTNU.

Disclosure statement

The authors declare that they have no conflict of interest.

Acronyms

AGO = atmospheric gas oil

CPM = cross-polarized microscopy

DOSY = diffusion ordered spectroscopy

DSC = differential scanning calorimetry

EVA = ethylene vinyl-acetate copolymer

HPLC = high-performance liquid chromatography

NMR = nuclear magnetic resonance

PA = polyacrylate

PB = polybutene

PE = polyethylene

PEP = poly(ethylene-propylene)

PFGSTE = pulsed field gradient stimulated echo

PPD = pour point depressant

PS = polystyrene

SEC = size exclusion chromatography

THF = tetrahydrofuran

WAT = wax appearance temperature

Figures and Tables

Table 1. PPD additives used in this study

PPD alias	Chemistry based on	Supplied by
PPD α	polycarboxylate (proprietary)	BASF, Germany
PPD β	PA, EVA (proprietary)	BASF, Germany
PPD τ	PS-block-poly(ethylene-ran-butylene)-block-PS	Sigmaaldrich, Norway
PPD Ω	EVA, 25% vinyl acetate	Sigmaaldrich, Norway

Table 2. Waxy oils used for PPD testing

Waxy oil alias	Amount of wax *wt.%*	Type of wax	Solvent oil
Model oil A	5	5405 Sasolwax	Primol 352
Model oil B	10	6805 Sasolwax	Primol 352
Model oil C	5	5405 Sasolwax	AGO
Crude oil	10	5405 Sasolwax	Light crude oil

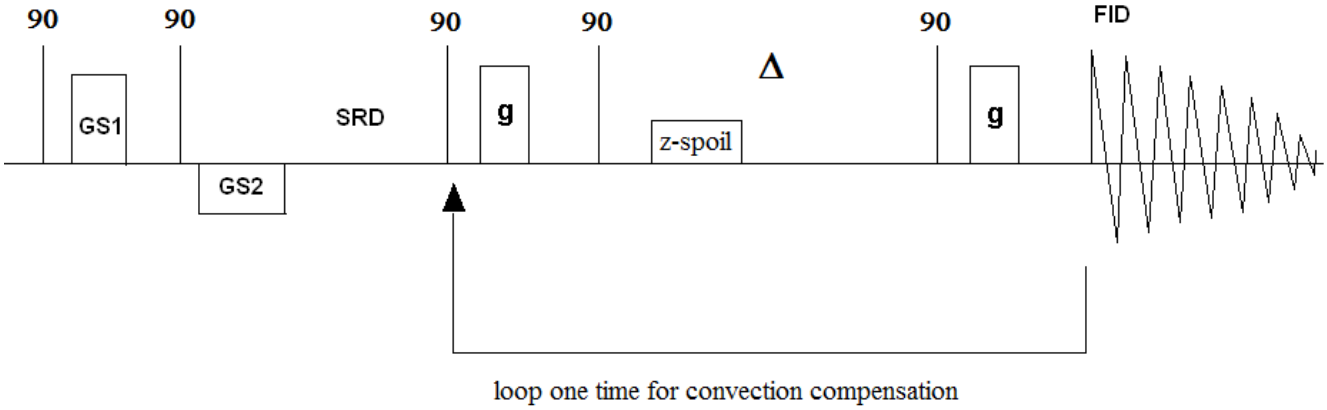

Figure 1. The rapid DOSY double PFGSTE experiment.

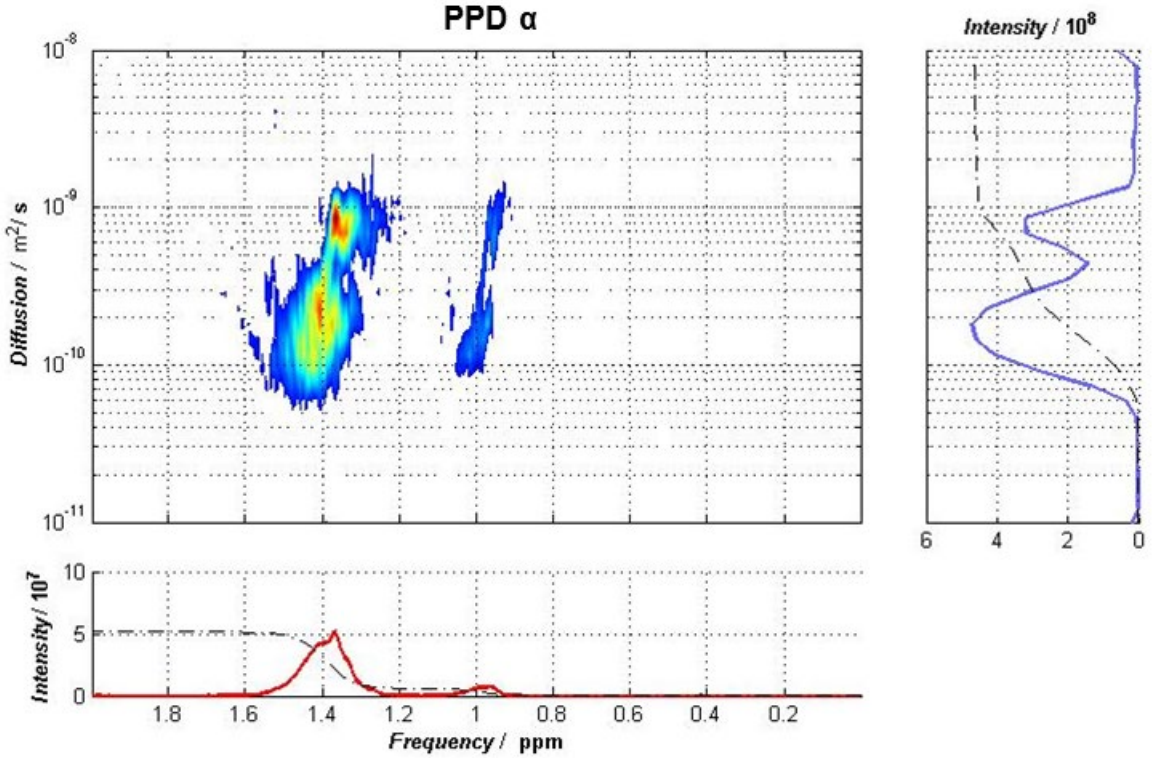

Figure 2. DOSY spectrum of 1000 ppm PPD α in deuterated toluene. The projection along the horizontal axis corresponds to the total frequency spectrum while the projection along the vertical axis is the distribution of diffusion coefficients.

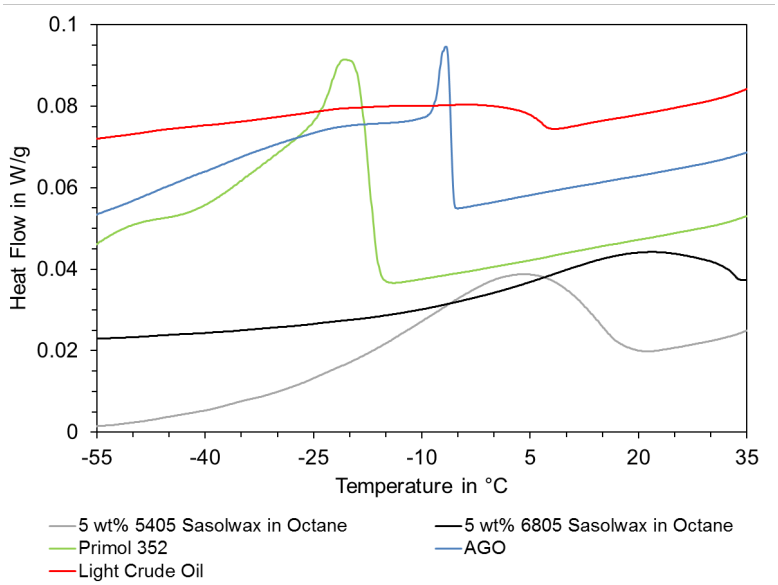

Figure 3. DSC heat flow per sample mass of waxy oils at a cooling rate of 5 °C/min. Graphs were shifted on the y-axis for better overview.

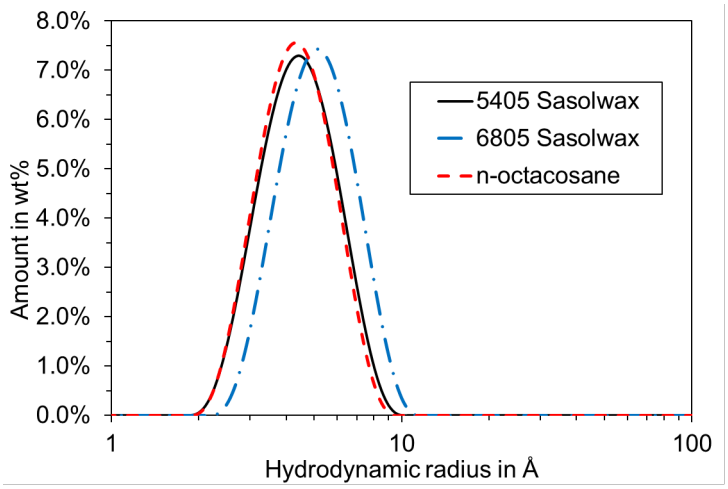

Figure 4. Hydrodynamic radius distribution (normalized by area) of 1000 ppm wax in deuterated toluene as determined by NMR-DOSY

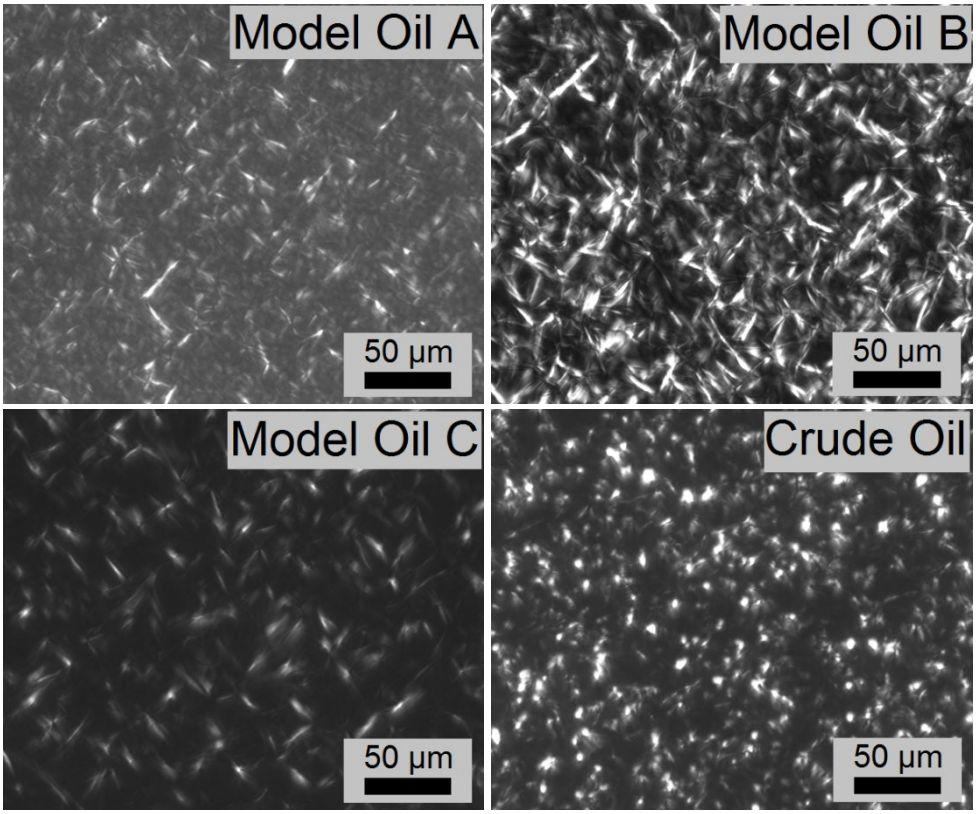

Figure 5. CPM images of different model oils and crude oil after isothermal equilibration at 5 °C (model oil A, model oil C, crude oil) or 20 °C (model oil B)

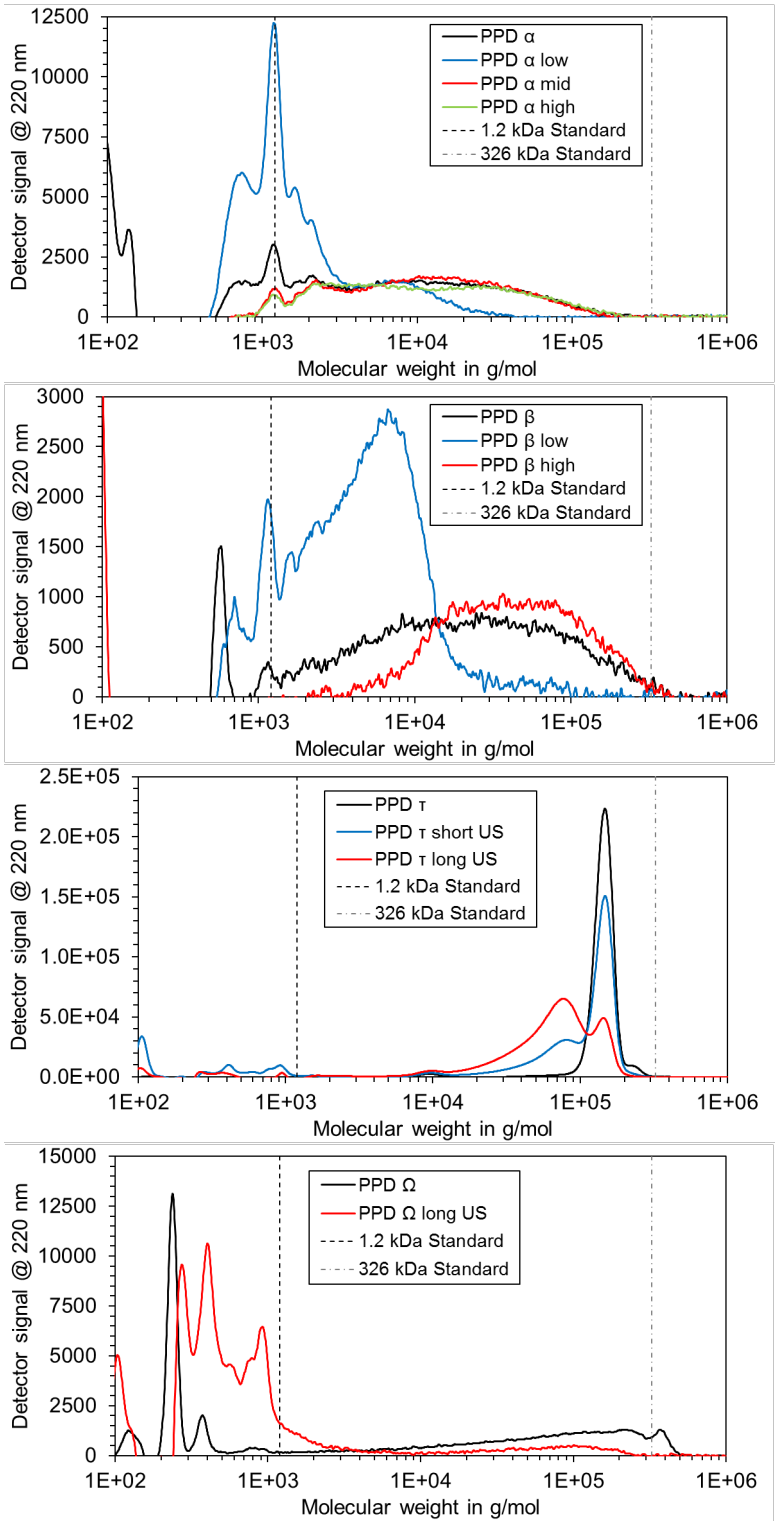

Figure 6. Molecular weight distribution in PS equivalent measured by HPLC-SEC

Table 3. Calculated average molecular weight in PS equivalent and polydispersity index

PPD alias	**Number Average Molecular Weight** *kDa*	**Weight Average Molecular Weight** *kDa*	**Polydispersity index** -
PPD α	17.70	65.59	3.71
PPD α low	2.76	8.52	3.09
PPD α mid	20.29	52.47	2.59
PPD α high	23.33	65.65	2.81
PPD β	43.46	128.46	2.96
PPD β low	6.53	18.01	2.76
PPD β high	65.37	132.60	2.03
PPD τ	142.72	150.58	1.06
PPD τ short US	103.64	133.63	1.29
PPD τ long US	69.47	100.49	1.45
PPD Ω	72.02	233.63	3.24
PPD Ω long US	7.29	110.50	15.17

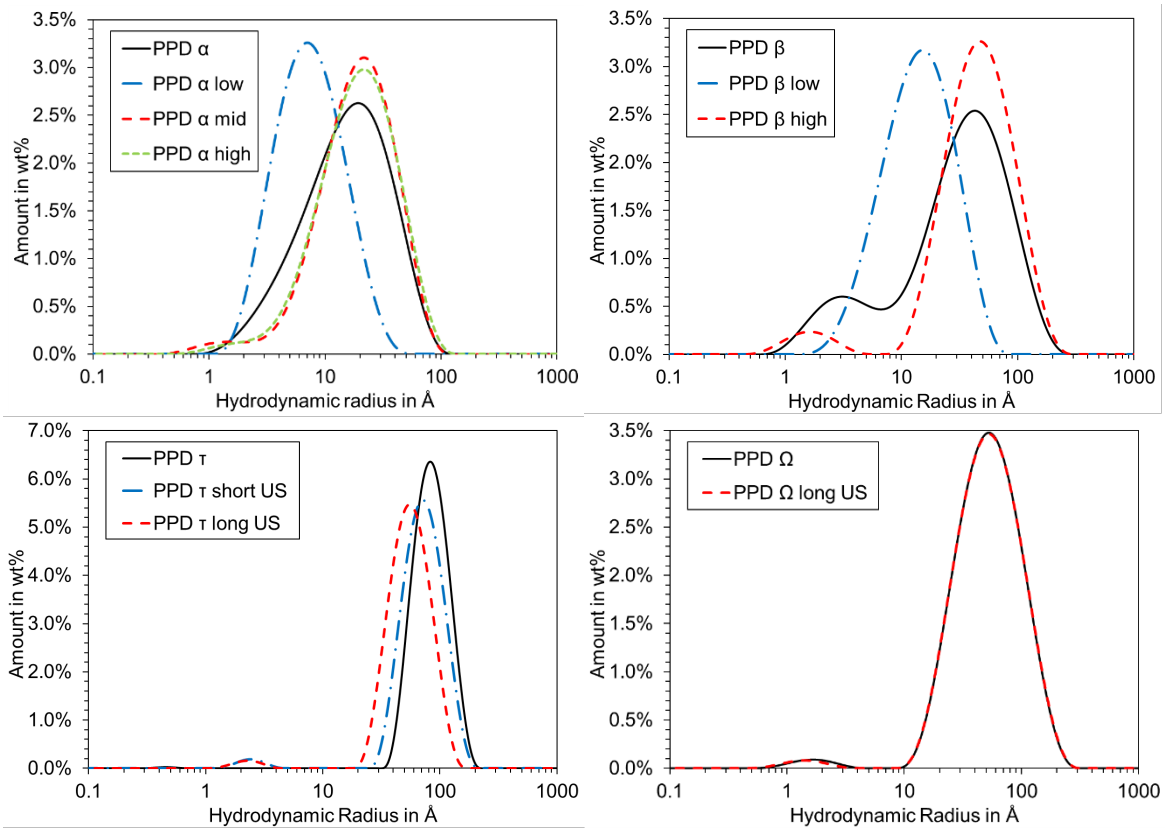

Figure 7. Hydrodynamic radius distribution (normalized by area) of 1000 ppm PPD in deuterated toluene as determined by NMR-DOSY

Table 4. Volume based average hydrodynamic radius of different PPDs and according sub-fractions

PPD alias	**Volume based average hydrodynamic radius** *Å*
PPD α	20.4
PPD α low	9.0
PPD α mid	23.2
PPD α high	23.9
PPD β	42.6
PPD β low	17.0
PPD β high	54.3
PPD τ	88.0
PPD τ short US	75.6
PPD τ long US	58.4
PPD Ω	61.9
PPD Ω long US	62.0

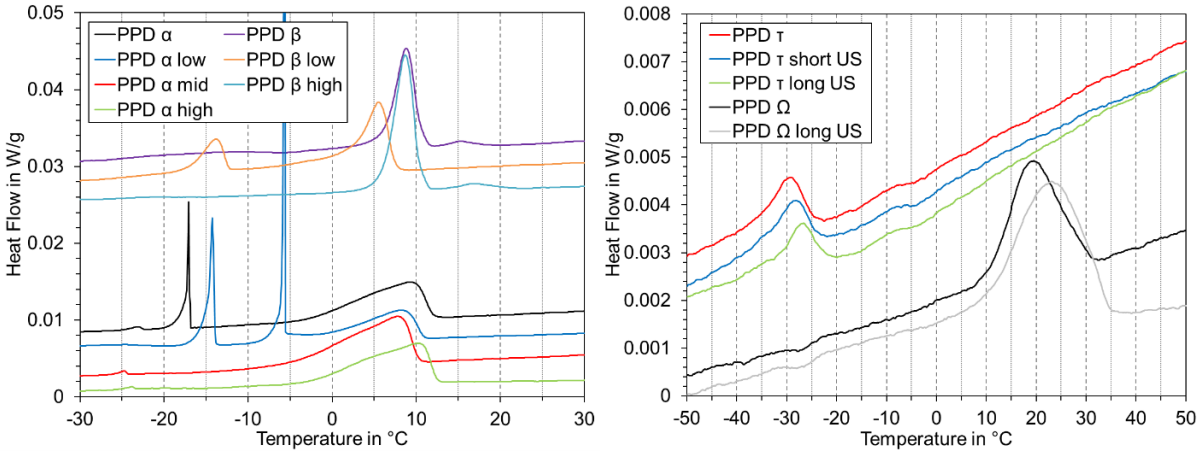

Figure 8. DSC heat flow of 5 wt% PPD in *n*-octane. Each graph was averaged over four measurements for improved signal to noise ratio. Graphs were shifted on the y-axis for better overview.

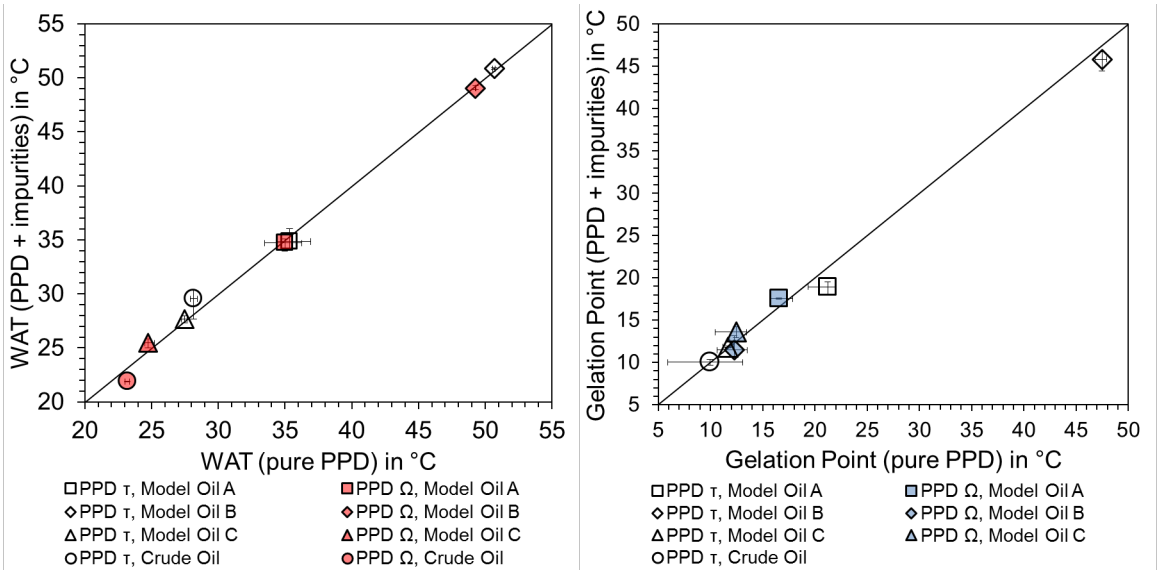

Figure 9. Comparison of WAT and gelation point for 500 ppm PPD τ or PPD Ω with or without impurities. Each point represents the average of at least four measurements, where error bars represent the maximum and minimum values obtained.

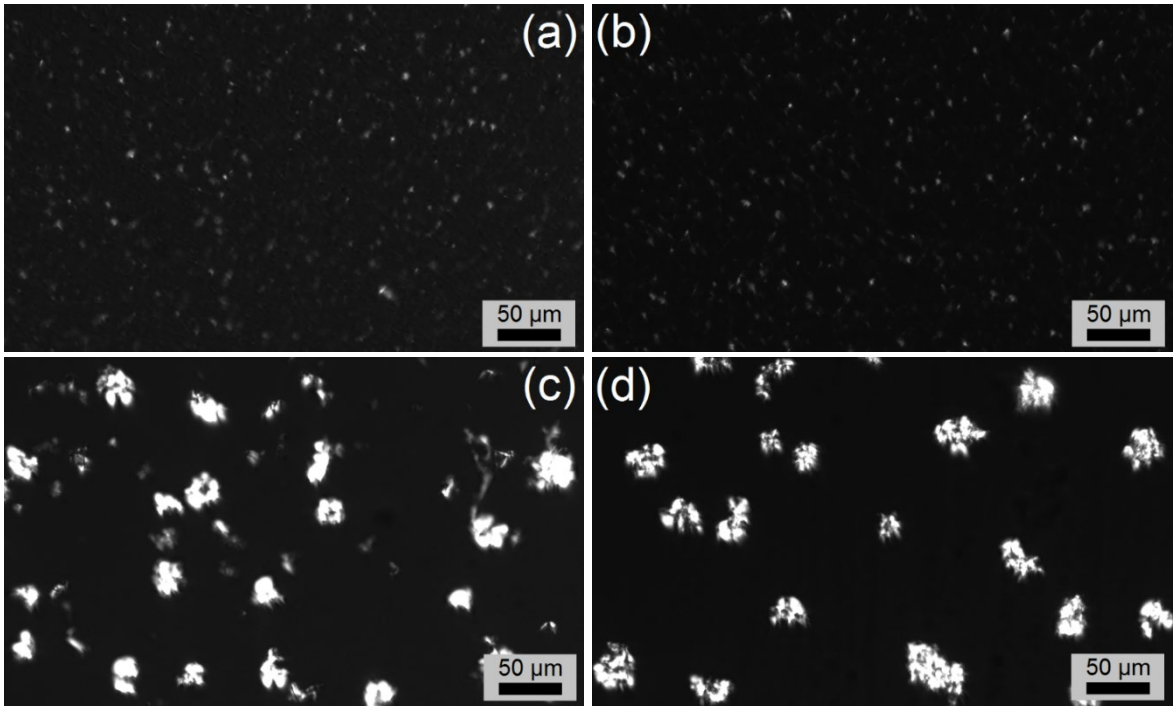

Figure 10. CPM images taken after isothermal equilibration at 20 °C of (a) 500 ppm PPD τ with impurities in crude oil, (b) 500 ppm pure PPD τ in crude oil, (c) 500 ppm PPD Ω with impurities in crude oil, and (d) 500 ppm pure PPD Ω in crude oil

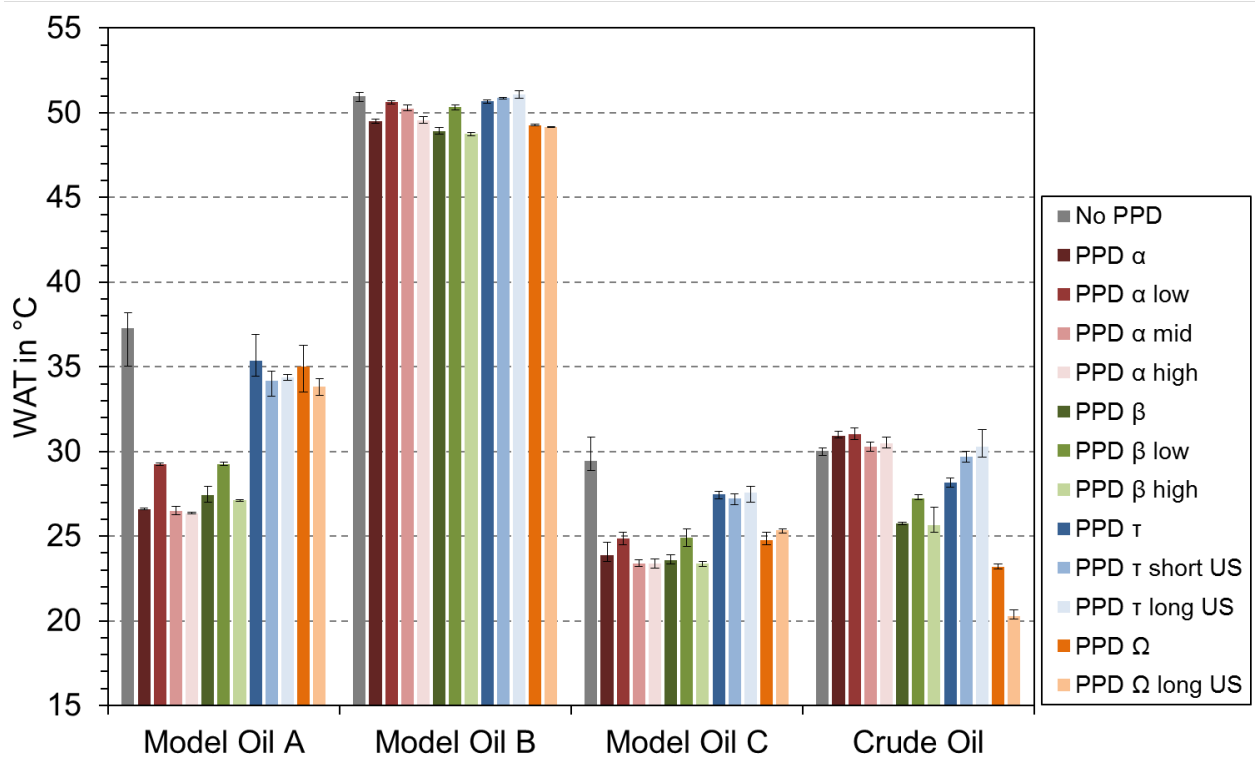

Figure 11. Average WAT computed from four DSC measurements of 500 ppm PPD in different waxy oils. Error bars represent the minimum and maximum WAT recorded for each sample.

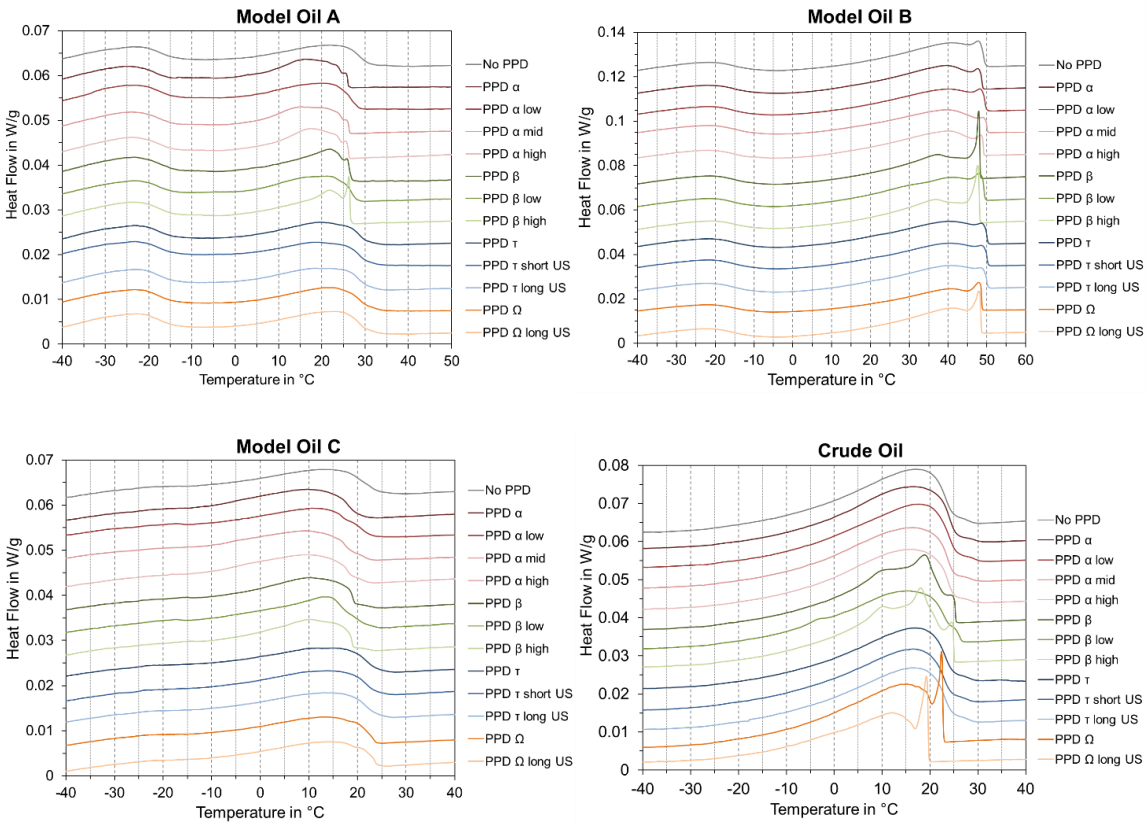

Figure 12. DSC heat flow per sample mass of 500 ppm PPD in different waxy oils.

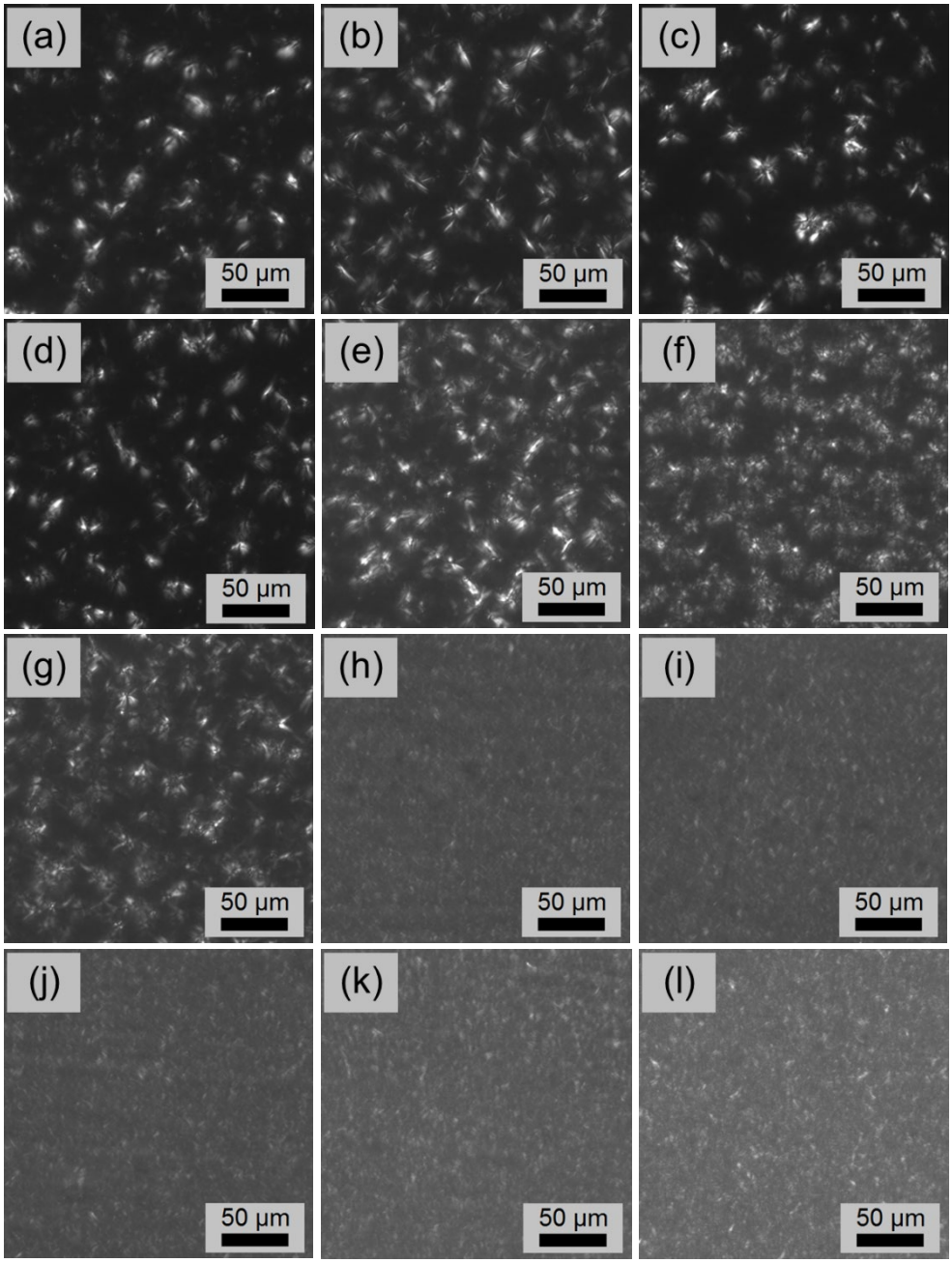

Figure 13. CPM images of 500 ppm PPD in model oil A after isothermal equilibration at 5 °C. The individual frames refer to (a) PPD α, (b) PPD α low, (c) PPD α mid, (d) PPD α high, (e) PPD β, (f) PPD β low, (g) PPD β high, (h) PPD τ, (i) PPD τ short US, (j) PPD τ long US, (k) PPD Ω, and (l) PPD Ω long US.

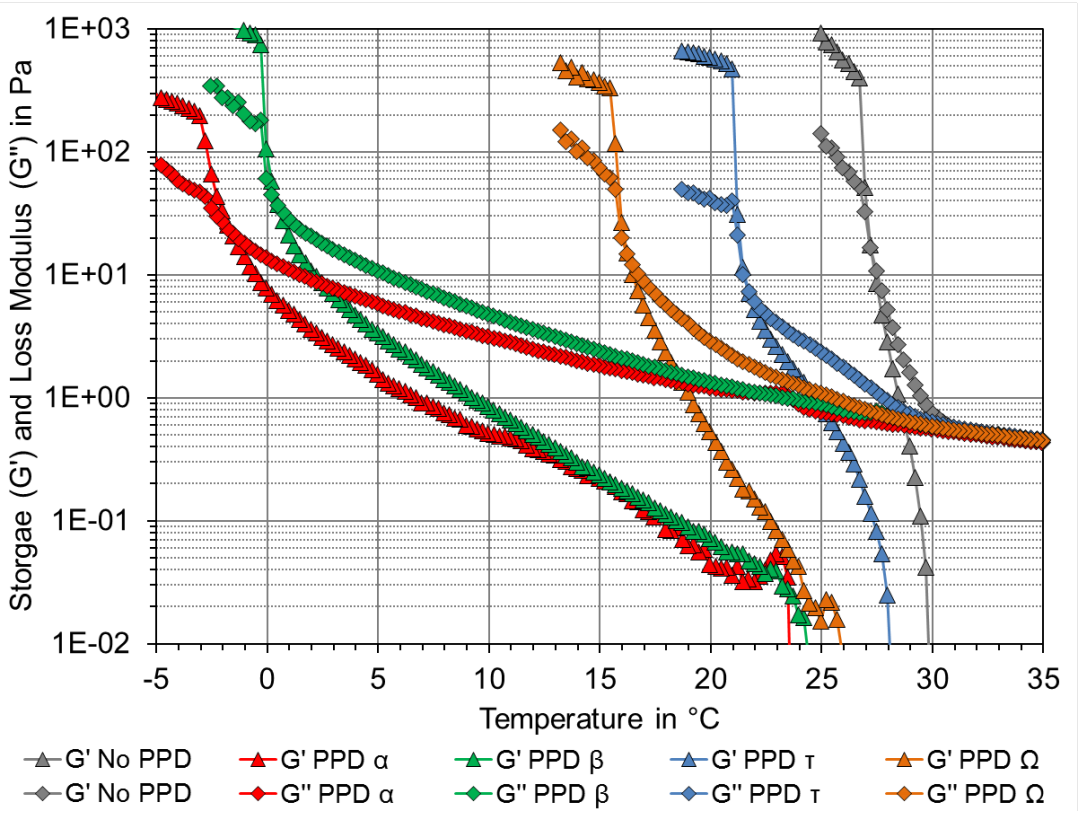

Figure 14. Exemplary data for storage (G') and loss modulus (G") during gelation point measurement.

The plotted data corresponds to measurements of 500 ppm PPD in model oil A.

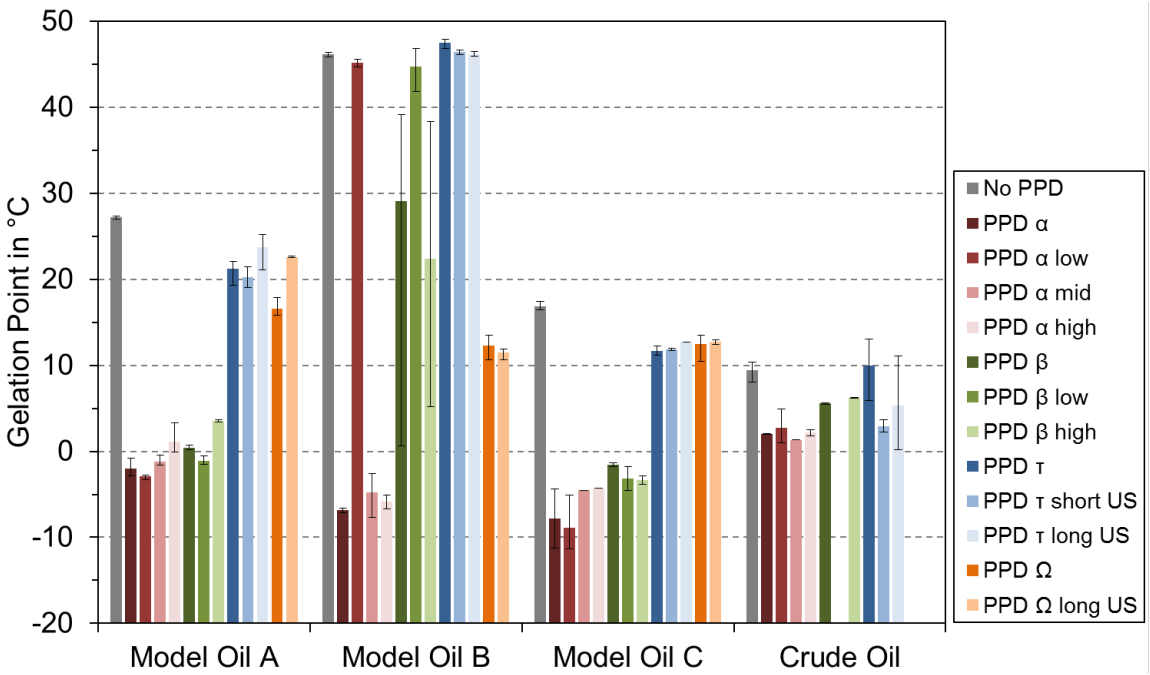

Figure 15. Gelation point averaged over at least four measurements of 500 ppm PPD in different waxy oils. Error bars mark the minimum and maximum gelation point temperature recorded for each sample. Measurements not displayed indicate that the gelation point was not reached at -20 °C and above.

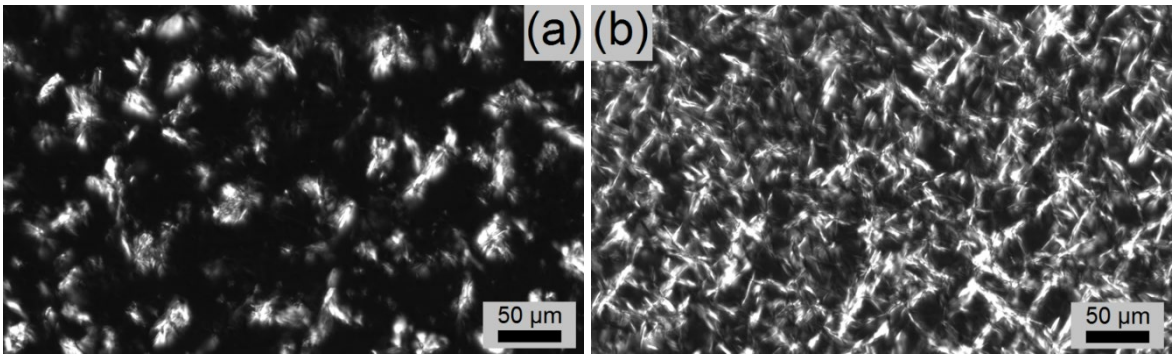

Figure 16. CPM images taken after isothermal equilibration at 20 °C of (a) 500 ppm PPD α in model oil B, and (b) 500 ppm PPD α low in model oil B

References

[1] Huang, Z.; Zheng, S.; Fogler, H. S., *Wax Deposition: Experimental Characterizations, Theoretical Modeling, and Field Practices*. CRC Press: Boca Raton (FL), USA, 2015.

[2] Zou, C.; Zhai, G.; Zhang, G.; Wang, H.; Zhang, G.; Li, J.; Wang, Z.; Wen, Z.; Ma, F.; Liang, Y.; Yang, Z.; Li, X.; Liang, K., Formation, distribution, potential and prediction of global conventional and unconventional hydrocarbon resources. *Petroleum Exploration and Development* **2015,** *42* (1), 14-28.

[3] Kelland, M. A., *Production chemicals for the oil and gas industry*. second ed.; CRC press: Boca Raton, 2014.

[4] Al-Yaari, M., Paraffin Wax Deposition: Mitigation and Removal Techniques. Society of Petroleum Engineers: 2011.

[5] Yang, F.; Zhao, Y.; Sjöblom, J.; Li, C.; Paso, K. G., Polymeric Wax Inhibitors and Pour Point Depressants for Waxy Crude Oils: A Critical Review. *Journal of Dispersion Science and Technology* **2015,** *36* (2), 213-225.

[6] Machado, A. L. d. C.; Lucas, E. F., Poly(Ethylene-co-Vinyl Acetate) (EVA) Copolymers as Modifiers of Oil Wax Crystallization. *Petroleum Science and Technology* **1999,** *17* (9-10), 1029-1041.

[7] Clarke, E. W., Crystal Types of Pure Hydrocarbons in the Paraffin Wax Range. *Industrial & Engineering Chemistry* **1951,** *43* (11), 2526-2535.

[8] Oschmann, H.-J. Das Kristallisationsverhalten von Paraffinen in Abhängigkeit von ihrer Zusammensetzung sowie seine Beeinflussung durch Paraffininhibitoren. PhD Thesis, Technische Universität Clausthal, Papierflieger, 1998.

[9] Geri, M.; Venkatesan, R.; Sambath, K.; McKinley, G. H., Thermokinematic memory and the thixotropic elasto-viscoplasticity of waxy crude oils. *Journal of Rheology* **2017,** *61* (3), 427-454.

[10] Standard Test Method for Pour Point of Petroleum Products. In *D97*, ASTM International, 2017.

[11] Zhao, Y.; Paso, K.; Kumar, L.; Safieva, J.; Sariman, M. Z. B.; Sjöblom, J., Controlled Shear Stress and Controlled Shear Rate Nonoscillatory Rheological Methodologies for Gelation Point Determination. *Energy & Fuels* **2013,** *27* (4), 2025-2032.

[12] Venkatesan, R.; Singh, P.; Fogler, H. S., Delineating the Pour Point and Gelation Temperature of Waxy Crude Oils. **2004**.

[13] Venkatesan, R.; Nagarajan, N. R.; Paso, K.; Yi, Y. B.; Sastry, A. M.; Fogler, H. S., The strength of paraffin gels formed under static and flow conditions. *Chemical Engineering Science* **2005,** *60* (13), 3587-3598.

[14] Venkatesan, R.; Östlund, J.-A.; Chawla, H.; Wattana, P.; Nydén, M.; Fogler, H. S., The Effect of Asphaltenes on the Gelation of Waxy Oils. *Energy & Fuels* **2003,** *17* (6), 1630-1640.

[15] Smith, P. B.; Ramsden, R. M. J., The Prediction Of Oil Gelation In Submarine Pipelines And The Pressure Required For Restarting Flow. In *SPE European Petroleum Conference*, Society of Petroleum Engineers: London, United Kingdom, 1978.

[16] Duffy, D.; Rodger, P., Wax inhibition with poly (octadecyl acrylate). *Physical Chemistry Chemical Physics* **2002,** *4* (2), 328-334.

[17] Zhang, J.; Zhang, M.; Wan, J.; Li, W., Theoretical Study of the Prohibited Mechanism for Ethylene/Vinyl Acetate Co-polymers to the Wax Crystal Growth. *The Journal of Physical Chemistry B* **2008,** *112* (1), 36-43.

[18] Monkenbusch, M.; Schneiders, D.; Richter, D.; Willner, L.; Leube, W.; Fetters, L. J.; Huang, J. S.; Lin, M., Aggregation behaviour of PE–PEP copolymers and the winterization of diesel fuel. *Physica B: Condensed Matter* **2000,** *276-278*, 941-943.

[19] Leube, W.; Monkenbusch, M.; Schneiders, D.; Richter, D.; Adamson, D.; Fetters, L.; Dounis, P.; Lovegrove, R., Wax-Crystal Modification for Fuel Oils by Self-Aggregating Partially Crystallizable Hydrocarbon Block Copolymers. *Energy & Fuels* **2000,** *14* (2), 419-430.

[20] Ashbaugh, H. S.; Guo, X.; Schwahn, D.; Prud'homme, R. K.; Richter, D.; Fetters, L. J., Interaction of Paraffin Wax Gels with Ethylene/Vinyl Acetate Co-polymers. *Energy & Fuels* **2005,** *19* (1), 138-144.

[21] Radulescu, A.; Schwahn, D.; Monkenbusch, M.; Fetters, L. J.; Richter, D., Structural study of the influence of partially crystalline poly(ethylene butene) random copolymers on paraffin crystallization in dilute solutions. *Journal of Polymer Science Part B: Polymer Physics* **2004,** *42* (17), 3113-3132.
[22] Pedersen, K. S.; Rønningsen, H. P., Influence of Wax Inhibitors on Wax Appearance Temperature, Pour Point, and Viscosity of Waxy Crude Oils. *Energy & Fuels* **2003,** *17* (2), 321-328.
[23] Wang, K.-S.; Wu, C.-H.; Creek, J. L.; Shuler, P. J.; Tang, Y., Evaluation of Effects of Selected Wax Inhibitors on Wax Appearance and Disappearance Temperatures. *Petroleum Science and Technology* **2003,** *21* (3-4), 359-368.
[24] Chen, W.; Zhao, Z.; Yin, C., The interaction of waxes with pour point depressants. *Fuel* **2010,** *89* (5), 1127-1132.
[25] Wei, B., Recent advances on mitigating wax problem using polymeric wax crystal modifier. *Journal of Petroleum Exploration and Production Technology* **2015,** *5* (4), 391-401.
[26] Wu, Y.; Ni, G.; Yang, F.; Li, C.; Dong, G., Modified Maleic Anhydride Co-polymers as Pour-Point Depressants and Their Effects on Waxy Crude Oil Rheology. *Energy & Fuels* **2012,** *26* (2), 995-1001.
[27] Yao, B.; Li, C.; Zhang, X.; Yang, F.; Sun, G.; Zhao, Y., Performance improvement of the ethylene-vinyl acetate copolymer (EVA) pour point depressant by small dosage of the amino-functionalized polymethylsilsesquioxane (PAMSQ) microsphere. *Fuel* **2018,** *220*, 167-176.
[28] Jing, G.; Sun, Z.; Tu, Z.; Bian, X.; Liang, Y., Influence of Different Vinyl Acetate Contents on the Properties of the Copolymer of Ethylene and Vinyl Acetate/Modified Nano-SiO2 Composite Pour-Point Depressant. *Energy & Fuels* **2017,** *31* (6), 5854-5859.
[29] Norrman, J.; Solberg, A.; Sjöblom, J.; Paso, K., Nanoparticles for Waxy Crudes: Effect of Polymer Coverage and the Effect on Wax Crystallization. *Energy & Fuels* **2016,** *30* (6), 5108-5114.
[30] Yang, F.; Paso, K.; Norrman, J.; Li, C.; Oschmann, H.; Sjöblom, J., Hydrophilic nanoparticles facilitate wax inhibition. *Energy & Fuels* **2015,** *29* (3), 1368-1374.
[31] Borthakur, A.; Chanda, D.; Dutta Choudhury, S. R.; Rao, K. V.; Subrahmanyam, B., Alkyl Fumarate−Vinyl Acetate Copolymer as Flow Improver for High Waxy Indian Crude Oils. *Energy & Fuels* **1996,** *10* (3), 844-848.
[32] Manka, J. S.; Ziegler, K. L., Factors Affecting the Performance of Crude Oil Wax-Control Additives. In *SPE Production and Operations Symposium*, Society of Petroleum Engineers: Oklahoma City, Oklahoma, 2001; p 7.
[33] Morris, K. F.; Johnson Jr, C. S., Diffusion-ordered two-dimensional nuclear magnetic resonance spectroscopy. *Journal of the American Chemical Society* **1992,** *114* (8), 3139-3141.
[34] Johnson Jr, C. S., Diffusion ordered nuclear magnetic resonance spectroscopy: principles and applications. *Progress in Nuclear Magnetic Resonance Spectroscopy* **1999,** *34* (3-4), 203-256.
[35] Provencher, S. W., A constrained regularization method for inverting data represented by linear algebraic or integral equations. *Computer Physics Communications* **1982,** *27* (3), 213-227.
[36] Jerschow, A.; Müller, N., Convection Compensation in Gradient Enhanced Nuclear Magnetic Resonance Spectroscopy. *Journal of Magnetic Resonance* **1998,** *132* (1), 13-18.
[37] Einstein, A., Über die von der molekularkinetischen Theorie der Wärme geforderte Bewegung von in ruhenden Flüssigkeiten suspendierten Teilchen. *Annalen der Physik* **1905,** *322* (8), 549-560.
[38] Ruwoldt, J.; Kurniawan, M.; Oschmann, H.-J., Non-linear dependency of wax appearance temperature on cooling rate. *Journal of Petroleum Science and Engineering* **2018,** *165*, 114-126.
[39] Chen, J.; Zhang, J.; Li, H., Determining the wax content of crude oils by using differential scanning calorimetry. *Thermochimica Acta* **2004,** *410* (1–2), 23-26.
[40] Paso, K.; Kompalla, T.; Oschmann, H. J.; Sjöblom, J., Rheological Degradation of Model Wax-Oil Gels. *Journal of Dispersion Science and Technology* **2009,** *30* (4), 472-480.
[41] Oliveira, G. E.; Mansur, C. R. E.; Lucas, E. F.; González, G.; de Souza, W. F., The Effect of Asphaltenes, Naphthenic Acids, and Polymeric Inhibitors on the Pour Point of Paraffins Solutions. *Journal of Dispersion Science and Technology* **2007,** *28* (3), 349-356.

[42] Yao, B.; Li, C.; Yang, F.; Sjöblom, J.; Zhang, Y.; Norrman, J.; Paso, K.; Xiao, Z., Organically modified nano-clay facilitates pour point depressing activity of polyoctadecylacrylate. *Fuel* **2016,** *166*, 96-105.
[43] Paso, K.; Senra, M.; Yi, Y.; Sastry, A. M.; Fogler, H. S., Paraffin Polydispersity Facilitates Mechanical Gelation. *Industrial & Engineering Chemistry Research* **2005,** *44* (18), 7242-7254.
[44] Bossard, F.; Moan, M.; Aubry, T., Linear and nonlinear viscoelastic behavior of very concentrated plate-like kaolin suspensions. *Journal of Rheology* **2007,** *51* (6), 1253-1270.